ARTICLES

Ultrafast Fluorescence Study on the Excited Singlet-State Dynamics of *all-trans*-Retinal

Satoshi Takeuchi and Tahei Tahara*

Institute for Molecular Science, Myodaiji, Okazaki 444, Japan

Received: September 10, 1996; In Final Form: February 24, 1997[⊗]

The femtosecond time-resolved fluorescence of *all-trans*-retinal in hexane was measured by using the fluorescence up-conversion method. It was found that the fluorescence consists of ultrafast ($\tau = 30 \pm 15$ fs and $\lambda_{max} \approx 430$ nm), fast ($\tau = 370 \pm 20$ fs and $\lambda_{max} \approx 440$ nm), and slow ($\tau = 33.5$ ps and $\lambda_{max} \approx 560$ nm) components. These three components were assigned to fluorescences from the ^1B_u, ^1A_g, and $^1n\pi^*$ states, respectively, which are successively populated during the relaxation process in the singlet manifold after photoexcitation. The oscillator strengths of the three excited singlet states were determined to be 1.0 (^1B_u), 0.024 (^1A_g), and 0.0018 ($^1n\pi^*$) on the basis of the obtained time-resolved fluorescence data. The state ordering in the singlet manifold, as well as quantitative characterization of the three low-lying excited singlet states, is discussed.

1. Introduction

Photochemistry of retinyl chromophores has been attracting much interest, especially in relation to their biochemical importance in photoreceptor proteins such as rhodopsin and bacteriorhodopsin.[1] The chromophore in rhodopsin, for example, is a protonated Schiff base of 11-*cis*-retinal bound to the protein opsin. It is known that a rapid *cis* → *trans* photoisomerization of this chromophore triggers the vision process which consists of a series of thermally induced bleaching reactions involving several kinds of intermediates.[2−4] The photoisomerization process, as well as excited state dynamics of the retinyl chromophore, has been extensively studied by time-resolved absorption and fluorescence spectroscopies using ultrashort optical pulses.[5−11]

While the protonated Schiff base of retinal is responsible for these biological functions, a free retinal itself has also been one of the central issues of photochemical studies because of its characteristic features in photoisomerization:[12] the photoisomerization from mono-*cis*-retinal takes place efficiently and predominantly yields *all-trans*-retinal, whereas the photoisomerization from *all-trans*-retinal is much less efficient and the major product is 13-*cis*-retinal.[13−17] Owing to the significant difference in the photoisomerization efficiency of *trans* and *cis* isomers, the photoisomerization of this molecule is sometimes called "one-way isomerization".[18,19] Time-resolved spectroscopy has been playing a crucial role in the elucidation of the mechanism and the dynamics of the photoisomerization of this molecule. Nanosecond and picosecond time-resolved spectroscopies such as UV−vis absorption,[12,20−24] infrared absorption,[25] spontaneous Raman,[26−30] and 2D-CARS[31] (CARS, coherent anti-Stokes Raman spectroscopy) have been applied to this molecule and afforded detailed information about the potential curves and dynamics of the excited state. Such time-resolved spectroscopic approaches, so far, have been mainly focused on the excited triplet state since the efficient isomerization from *cis* to *trans* takes place in the triplet manifold.[18] However, recent nanosecond time-resolved infrared absorption study suggested that the photoisomerization from *trans* to *cis* proceeds not in the excited triplet state but in the excited singlet state.[25] Therefore, it is evident that the knowledge about the excited singlet-state dynamics is also indispensable for full understanding of the retinal photochemistry.

In the singlet manifold of retinal, an optically forbidden state of A_g character is located near the optically allowed ^1B_u state, as usually found for conjugated polyenes.[32,33] In addition to this ^1A_g state, there also exists another low-lying optically forbidden excited singlet state, $^1n\pi^*$ state, in polyene aldehydes like retinal. These three excited singlet states, the ^1B_u, ^1A_g, and $^1n\pi^*$ states, are located closely to one another and can participate in the ultrafast excited state dynamics of retinal. It is also known that the photochemical properties of retinal are greatly influenced by relative ordering of the three excited singlet states,[34−36] as manifested by, for instance, solvent-dependent quantum yield of intersystem crossing.[12,37] Therefore, it is highly desirable to clarify the properties and energies of these three excited singlet states in addition to their dynamics.

One of the authors of this paper and Hamaguchi measured picosecond time-resolved fluorescence spectra of *all-trans*-retinal with a 8-ps time resolution and found a sub-picosecond decay component in addition to the component ascribable to the S_1 fluorescence.[38] This finding clearly indicated that ultrafast processes are involved in retinal photochemistry and that femtosecond time-resolution is required to investigate the dynamics of the excited singlet state(s) of retinal. It was only very recently that the femtosecond time-resolved visible absorption spectroscopy was applied to retinal itself.[39]

In this paper we report our femtosecond up-conversion study on the dynamics of the excited singlet states of *all-trans*-retinal in nonpolar solvent. The advantage of time-resolved fluorescence spectroscopy over time-resolved absorption spectroscopy lies in the fact that fluorescence originates from the optical

* To whom correspondence should be addressed: TEL +81-564-55-7391, FAX +81-564-54-2254, E-mail, tahara@ims.ac.jp.

[⊗] Abstract published in *Advance ACS Abstracts,* April 1, 1997.

S1089-5639(96)02765-X CCC: $14.00 © 1997 American Chemical Society

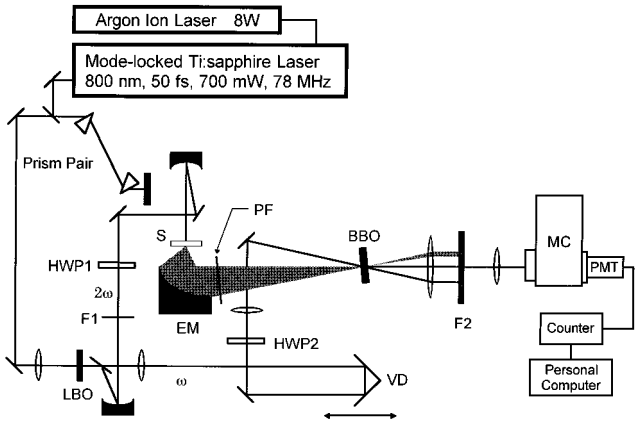

Figure 1. Schematic diagram of the experimental setup used for the fluorescence up-conversion measurements. S, sample; EM, elliptic mirror; PF, polarizing film; F1 and F2, optical filters; HWP1 and HWP2, half-wave plates for 400 and 800 nm, respectively; VD, variable delay line; MC, monochromator; PMT, photomultiplier.

transition between the "well-known" ground state and the excited state in question. Thus time-resolved fluorescence spectroscopy can afford unique information not only about the dynamics but also other properties of the excited singlet states such as their energies and oscillator strengths, which are not obtainable from time-resolved absorption data.

2. Experimental Section

2.1. Setup. The experimental setup used for the fluorescence up-conversion measurements is shown in Figure 1. The light source is a mode-locked Ti:sapphire laser (Coherent, MIRA 900F) pumped by an 8 W all-lines radiation of an Ar^+ laser (Coherent, INNOVA 310). The oscillator produces a 78 MHz pulse train with ≥700 mW average power in a tunable range of 760−840 nm. The lasing wavelength was fixed at $\lambda = 800$ nm in the present up-conversion measurements. An extracavity prism sequence is employed for group-velocity-dispersion (GVD) compensation to obtain the shortest possible pulses. An interferometric autocorrelation trace of the output pulses after the prism sequence indicated a chirp-free pulse with the duration as short as 50 fs.

The second-harmonic pulse ($\lambda = 400$ nm, ≈15 mW, $\tau_p \approx$ 140 fs) is generated in a 1 mm-thick LiB_3O_5 (LBO) crystal ($\theta = 90°$, $\phi = 32°$) and it is used as the pump pulse for photoexcitation. The residual fundamental pulse (500 mW) is used as the gate pulse in the up-conversion process. The pump pulse is focused on a thin filmlike jet stream (300 μm thickness) of the sample solution after passing through a variable-transmittance neutral-density filter. At the sample point, the maximum average power of the pump flux is 10 mW, and its beam diameter is ≈ 120 μm as measured with the knife-edge method. The fluorescence emitted from the sample is collected and focused into a 0.5-mm-thick β-BaB_2O_4 (BBO) mixing crystal ($\theta = 40°$) by an aluminum-coated elliptic mirror. The focal lengths of the mirror are 50 mm (for fluorescence collection) and 150 mm (for fluorescence focusing). The elliptic mirror is used in place of a lens because it is free from any spherical/chromatic aberrations and the GVD effect. A film polarizer (0.75 mm thick) is placed in between the elliptic mirror and the mixing crystal so that the vertically polarized, i.e., parallel to the gate polarization, component of the fluorescence is selected to be up-converted. The average transmittance of the polarizer for natural light is 40% in the visible region. The fluorescence detection at the magic angle is achieved by rotating the pump polarization with a half-wave plate. The

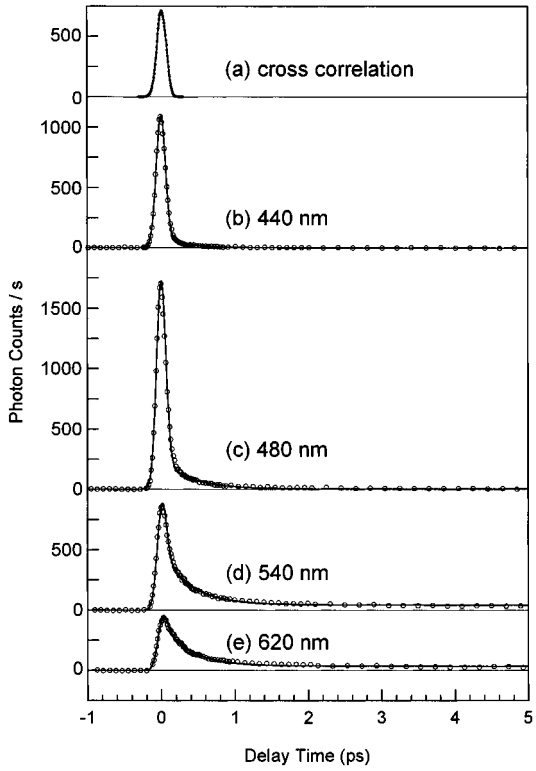

Figure 2. Up-converted fluorescence decay signals obtained from *all-trans*-retinal in hexane (1.2×10^{-3} mol dm^{-3}, 400 nm excitation). Cross-correlation trace between the gate pulse and the pump pulse (a), and fluorescence decays of *all-trans*-retinal at 440 (b), 480 (c), 540 (d), and 620 nm (e). The open circles are experimental data points, and the solid curves are results of the fitting analysis (see text). The instrumental time resolution given by the fwhm of the cross-correlation trace is 150 fs.

fluorescence and the gate pulse interact noncollinearly in the mixing crystal, and the crossing angle between the two is about 10°. The fluorescence wavelength to be up-converted is selected by changing the phase-matching angle of the mixing crystal. The up-converted signal is spatially and spectrally separated from the other lights (fluorescence itself, gate pulse, and unphase-matched second harmonic of the gate pulse) by using a combination of an iris, an optical filter (HOYA, U34), and a 0.32-m monochromator (Jobin Yvon, HR-320). The signal is detected by a photon-counting photomultiplier (Hamamatsu, H6180-01) with a gated photon counter (Stanford Research Systems, SR400). The spectral resolution of the up-conversion measurements ranges from ±3 to ±4 nm in the fluorescence wavelength from 420 to 640 nm.[40] The time resolution of the measurements is estimated as $\tau_{cross} = 150$ fs from the full width at half maximum (fwhm) of the cross-correlation trace between the pump and the gate pulses (Figure 2a).

The stationary fluorescence spectrum of the sample solution was measured with the same apparatus as used for the up-conversion measurements. The fluorescence collected by the elliptic mirror is not gated but directly introduced to the monochromator. The grating in the monochromator is motor driven with ±0.2 nm accuracy, and the spectral resolution of the measurements is about 2 nm. The fluorescence was detected with the magic angle configuration. The spectral sensitivity of the detection system was examined by using a standard halogen lamp with a 3124 K color temperature.

2.2. Sample. *all-trans*-Retinal was purchased from Sigma Chemical Co. and was used without further purification. It had been kept in a dark freezer, and was treated carefully under deep red light. Hexane (HPLC grade) was purchased from

Wako Pure Chemical Co. and was used as received. Spectroscopic-grade hexane was also used, but it did not make any difference in the experimental data. A fresh sample solution was prepared for each fluorescence decay measurement.

2.3. Excitation Condition. In the present study, a special attention has been paid to the excitation condition because *all-trans*-retinal undergoes photoisomerization and photoproducts might affect the experimental data. A quantitative consideration on the experimental condition is described in the following in order to show that the contribution of photoproducts to the obtained data is negligibly small.

The 78 MHz pump pulse train with 10 mW average power was focused in the 120-μm-diameter spot, yielding a peak power density of 8.1×10^{10} Wm^{-2}, or photon number density of $F_N = 1.6 \times 10^{29}$ m^{-2} s^{-1}. The mean time for one retinal molecule to absorb a photon under this pump photon flux is calculated as $\tau_{ex} = 1/(F_N\sigma) \approx 800$ ps using the absorption cross section of *all-trans*-retinal at 400 nm: $\sigma \approx 7.6 \times 10^{-21}$ m^2. Since the pump pulse duration τ_p is as short as 140 fs, retinal molecules need $\tau_{ex}/\tau_p = 5.7 \times 10^3$ pump pulses, or 73 μs, to be photoexcited once.

The sample solution is circulated with a flowing speed of 1.4 ml s^{-1}, or $\approx$ 160 cm s^{-1}, at the jet position, which means that retinal molecules pass through the irradiated area (120 μm diameter) with a transit time of $\tau_t = 75$ μs. Since this transit time is comparable to the time required for the photoexcitation (73 μs), each retinal molecule is excited only once while it passes through the irradiated volume.

The width of the jet stream (3 mm) is much larger than the pump spot size (120 μm), so that only 4% (=120 μm/3 mm) of the sample volume has experienced photoexcitation even if all sample solution is once circulated. The photoproduct (mainly 13-*cis* isomer) is produced with the quantum yield as low as 0.1.[13−17,20] Consequently, even with the longest measurement time of $\approx$ 700 s, in which the sample solution is circulated at most six times, the amount of the photoproduct does not exceed 2.4% (=4% × 0.1 × 6).

The above estimation which shows that the amount of the photoproduct is very small is supported by the following two experimental observations. (1) The absorption spectra of the sample solution before and after the measurement agreed with each other with deviations less than 1% for wavelength region of 300−450 nm and 2% for 220−300 nm. (2) The pump power change, which should change the amount of the photoproduct, did not affect the observed fluorescence decay as shown later.

3. Results and Discussion

3.1. Fluorescence Decay. The fluorescence decays at four different wavelengths obtained from hexane solution (1.2×10^{-3} mol dm^{-3}) are shown in Figure 2. The pump wavelength was 400 nm, and the average pump power was 10 mW. The measurement was made at room temperature. The up-converted signal was counted for 4−8 s at each delay time. The maximum signal count rate was as high as 1700 counts s^{-1} while the dark level was typically 5 counts s^{-1}. As clearly seen in this figure, the observed fluorescence decays are not single exponential, and their feature varies significantly with the change in the fluorescence wavelength. The fluorescence decay at 440 nm looks quite similar to the cross-correlation trace, indicating that the major portion of the fluorescence vanishes with a time constant much shorter than the time resolution (150 fs). In addition to this major "ultrafast" component, there exists the second "fast" component which can be recognized as a weak tail at early delay times. The second fluorescence component

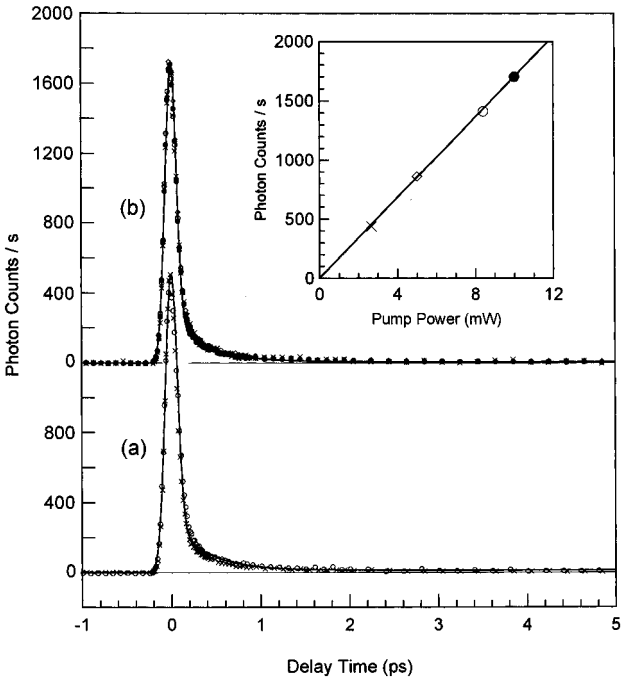

Figure 3. Signal decays obtained from *all-trans*-retinal in hexane (1.2×10^{-3} mol dm^{-3}; 400 nm excitation) under different experimental conditions. (a) Normalized signal decays at 480 nm with (○) and without (×) a cutoff filter which transmits only the longer wavelength light than 420 nm. (b) Normalized signal decays at 480 nm obtained with the pump powers of 2.7 (×), 5.0 (◇), 8.4 (○), and 10 mW (●). Inset: the pump power dependence of the peak signal intensities around the time origin.

becomes dominant with increase in the fluorescence wavelength. In the fluorescence decays at 540 and 620 nm, the third "slow" component appears, which is seen as an almost constant signal in the measured time range. These data indicate that the observed fluorescence decay consists of the three components, the ultrafast, the fast, and the slow components.

When we found the ultrafast component in the observed decay, we, at first, suspected that it might arise from some experimental artifacts such as an unphase-matched up-converted pump pulse. In order to check this point, we placed a cutoff filter (HOYA, L42, 2.5 mm thickness) in the fluorescence path before the mixing crystal, and measured signal decays at 480 nm. The filter optically blocks the scattering of the pump pulse and transmits only the light whose wavelength is longer than 420 nm. The signal decays obtained with and without the cutoff filter are compared in Figure 3a. The two decays are identical to each other, although a small difference attributable to the GVD effect by the filter is recognized at early delay times. This indicates that *the 480-nm light, not the scattering of the pump pulse at 400 nm*, was certainly up-converted. A nonlinear frequency-broadened short pulse generation such as white continuum generation might contribute to the ultrafast component. However, this possibility was also ruled out by the experiment for the pump power dependence. Figure 3b shows normalized signal decays at 480 nm measured with four different pump powers ranging from 2.7 to 10 mW. The obtained data shows that the signal decay is *independent of the pump power* and that the peak counts around the time origin exhibit *linear* dependence on the pump power (deviations less than 3%). This indicates that any nonlinear artifacts do not contribute to the observed signal. It is concluded that the signal decays shown in Figure 2 come solely from the intrinsic fluorescence of the sample solution.

In a previous paper,[38] Tahara and Hamaguchi measured picosecond time-resolved fluorescence of *all-trans*-retinal with use of a highly sensitive streak camera system with a 8 ps time-resolution and found two components in the observed fluorescence. The decay of the faster component was not time resolved owing to the limitation of the time resolution, and its lifetime was inferred to be shorter than 1 ps (the sub-picosecond component). The decay of the other slow component was clearly time-resolved, and the lifetime was determined as 33−34 ps from the streak traces up to 100 ps. The fluorescence up-conversion system used in the present study affords the time resolution as good as 150 fs, which is more than 50 times better than that of the streak camera employed in the previous work. The improved time resolution reveals that the subpicosecond component observed in the previous work, in reality, consists of two components, i.e., the ultrafast and the fast components. The third slow component is assignable to the 33−34-ps component already found in the previous work. The two time-resolved fluorescence studies covering femtosecond−picosecond time region show that three fluorescing states are involved in the relaxation process following the photoexcitation of *all-trans*-retinal.

Assuming a cascaded population relaxation for the three fluorescing states, the fitting analysis on the observed fluorescence decays was carried out based on the following functional form:

$$R(t) = a_0\delta(t) + a_1 e^{-t/\tau_1} + a_2(e^{-t/\tau_2} - e^{-t/\tau_1})$$
$$= A_0\delta(t) + A_1 e^{-t/\tau_1} + A_2 e^{-t/\tau_2} \quad (1)$$

with $a_0 = A_0$, $a_1 = A_1 + A_2$, and $a_2 = A_2$. In this formula, the ultrafast component is represented with the δ-function, because it decays much faster than the time resolution. The lifetime of the slow component τ_2 was fixed to 33.5 ps, and the fitting was made to a convoluted form, $C(t)\otimes R(t)$, searching for the best τ_1, A_0, A_1, and A_2 values by using the least-squares procedure. The following functional form was adopted as a normalized instrumental response:

$$C(t) = \frac{1}{\sqrt{\pi}T_c} e^{-t^2/T_c^2} \quad \text{with } T_c \equiv \frac{\tau_{cross}}{2\sqrt{\ln 2}}, \quad \int_{-\infty}^{\infty} C(t)\,dt \equiv 1 \quad (2)$$

The results of the fitting are shown with solid curves in Figure 2. The calculated curves successfully reproduce the observed fluorescence decays, except for the slight deviation found at very early delay times. This deviation is due to a finite lifetime of the ultrafast component. Replacing the δ-function by $(1/\tau_0)\exp(-t/\tau_0)$ in formula 1 and taking the finite lifetime of a few tens of femtoseconds, the deviation seemed to be corrected satisfactorily. As clearly seen in Figure 4, the calculated curve with $\tau_0 = 30$ fs gave the best fit to the experimental data, and we evaluated the lifetime of the ultrafast component to be 30 $\pm$ 15 fs.[41] The lifetime of the second fast component τ_1 obtained at each fluorescence wavelength showed good agreement, and it was determined as 370 $\pm$ 20 fs.

3.2. Fluorescence Spectra. The coefficients $a_0(\lambda)$, $a_1(\lambda)$, and $a_2(\lambda)$ determined by the fitting analysis include spectral information of the three decay components. However, in order to obtain fluorescence spectra from these values, we have to normalize these coefficients, because the signal intensity detected at each wavelength is significantly affected by the up-conversion efficiency. Thus, we measured the stationary fluorescence spectrum, and used it for the normalization of the up-converted fluorescence signals.

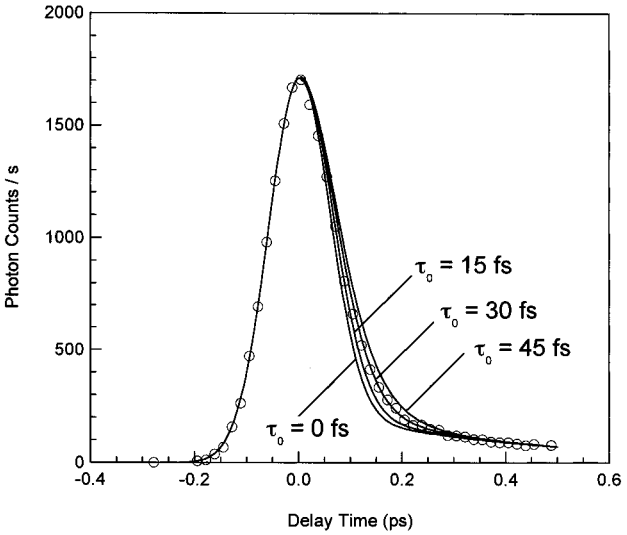

Figure 4. Comparison of the fluorescence decays at 480 nm (open circles) and the calculated curves (solid curves) with four different lifetimes of the ultrafast component $\tau_0 = 0$, 15, 30, and 45 fs. The signal-intensity fluctuation is $\pm$ 10 counts s^{-1}, and it is smaller than the size of the open circles.

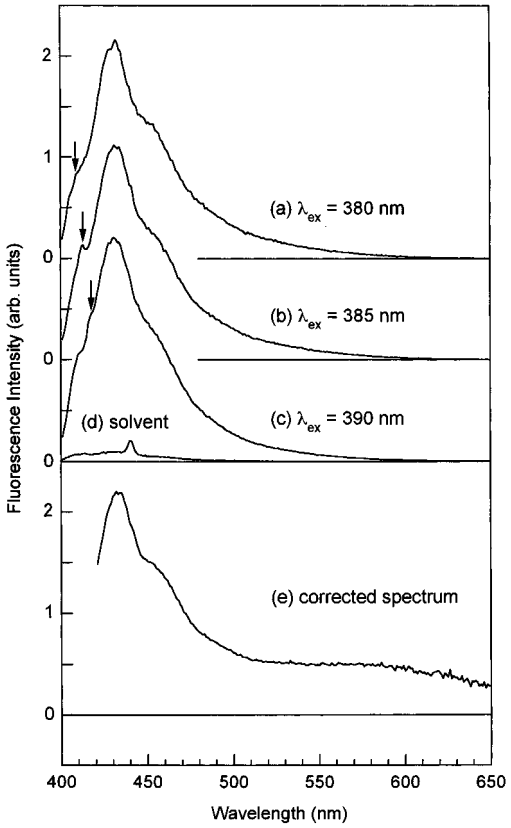

Figure 5. Time-integrated stationary fluorescence spectra of *all-trans*-retinal in hexane (1.2×10^{-3} mol dm^{-3}). (a−c) Raw fluorescence spectra obtained with excitation at 380, 385, and 390 nm, respectively. The arrows indicate the resonance Raman bands due to *all-trans*-retinal. (d) Scattered light spectrum obtained from the solvent excited at 390 nm. (e) Stationary fluorescence spectrum after the sensitivity correction of the detection system.

The stationary fluorescence spectra obtained with photoexcitation at 380, 385, and 390 nm are shown in Figure 5. The fluorescence of *all-trans*-retinal exhibits an intensity maximum at ~430 nm with a broad shoulder around 455 nm. The obtained spectra are completely different from the reported fluorescence spectrum of hydrogen-bonded *all-trans*-retinal ($\lambda_{max} \approx 520$ nm[37,42]), implying that the sample solution is free from

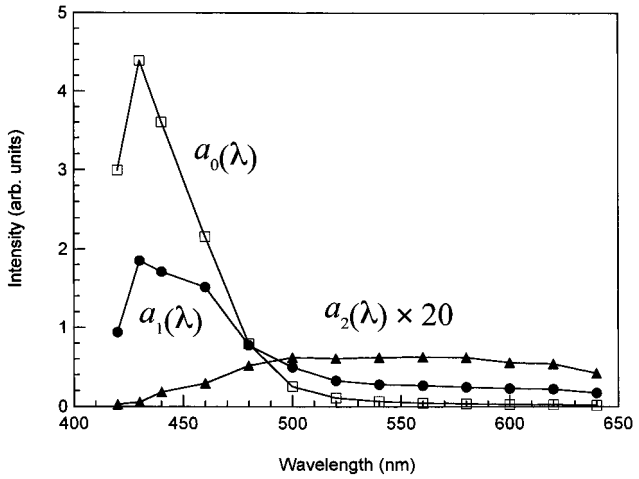

Figure 6. Fluorescence spectra corresponding to the ultrafast (□), fast (●), and slow (▲) decay components.

contaminations of proton-donating water and/or alcohols. The following two points are probably worth mentioning for the spectra shown here. First, the sensitivity of the detector is low for the wavelength region longer than 550 nm so that it might cause some intensity uncertainty in the spectra of this region. Secondly, these spectra contain small contribution of Raman scattering. The scattered light spectrum obtained from the solvent is shown in Figure 5d, in which a Raman band due to the C−H stretching vibration of hexane is clearly found with a featureless background arising from a stray light of the excitation line. In addition, resonance Raman bands due to *all-trans*-retinal can be recognized in the fluorescence spectra, for example, as indicated by arrows in Figure 5a−c. The fluorescence of *all-trans*-retinal is so weak that these Raman bands cannot be neglected. The fluorescence spectra were measured also with other excitation wavelengths including 395 and 400 nm. All excitation wavelengths gave the identical spectra except for the Raman contributions which shift in accordance with the change in the excitation wavelength.

Using the stationary fluorescence spectrum obtained after the detection-sensitivity correction (Figure 5e), the intensity normalization of the up-converted signal can be made on the basis of the following formula:

$$S \propto \int_{-\infty}^{\infty} C(t) \otimes R(t)\, \mathrm{d}t = \int_{-\infty}^{\infty} R(t)\, \mathrm{d}t$$
$$= A_0 + A_1\tau_1 + A_2\tau_2$$
$$= a_0 + (a_1 - a_2)\tau_1 + a_2\tau_2 \qquad (3)$$

This formula comes from the fact that the time integration of the up-converted fluorescence decay signal ($C(t) \otimes R(t)$) yields a value proportional to the stationary fluorescence intensity (S) at each wavelength. We measured the up-converted fluorescence decays at 13 wavelengths and determined the coefficients $a_0(\lambda)$, $a_1(\lambda)$, and $a_2(\lambda)$ by the fitting analysis. The normalized coefficients are plotted in Figure 6 against the fluorescence wavelength. They represent fluorescence spectra of the three decay components. The fluorescence spectrum of the ultrafast component $a_0(\lambda)$ is sharply peaked at 430 nm, while that of the second fast component $a_1(\lambda)$ shows a broader peak around 440 nm. The fluorescence spectrum due to the slow component $a_2(\lambda)$ is much weaker than the spectra of other two and exhibits an intensity maximum around 560 nm. These three spectra show a sequential red shift. This fact strongly supports that the three fluorescing states participate in the cascaded relaxation process taking place after the photoexcitation.

In the previous paper,[38] the fluorescence intensity maximum of the sub-picosecond component, which corresponds to the ultrafast and the fast components in the present study, was reported to be around 470 nm. This value was obtained from the spectral data for the wavelength region of 450−650 nm. The present study covering wider wavelength region has revealed that the real intensity maximum is located at ∼430 nm. The reported peak around 470 nm probably corresponds to the shoulder peak, which is clearly seen in the stationary fluorescence spectrum in Figure 5e. The fluorescence spectrum of the slow component obtained from the present up-conversion measurements is in very good agreement with the reported spectrum obtained with a streak camera.

The normalized coefficients, i.e., the fluorescence spectra shown in Figure 6, also contain information on radiative decay rates (inverse of radiative lifetimes), or oscillator strengths. The radiative decay rates of the three fluorescing states are proportional to the quantities F_0, F_1, and F_2 which are defined as

$$F_0 \equiv \int_{-\infty}^{\infty} (1/\tau_0) a_0(\nu)\, \mathrm{d}\nu \quad \text{and} \quad F_i \equiv \int_{-\infty}^{\infty} a_i(\nu)\, \mathrm{d}\nu \qquad (i = 1, 2) \quad (4)$$

The factor of $1/\tau_0$ with the lifetime of $\tau_0 = 30$ fs is introduced in the definition of F_0 because the δ-function representing the ultrafast decay component in formula 1 can be replaced by $(1/\tau_0) \exp(-t/\tau_0)$. In order to calculate these values based on the obtained spectra, we represented the spectra in the ν-space by using a relation $a_i(\nu) = \lambda^2 a_i(\lambda)$ and then replaced each spectrum with the best fitted Lorentzian function:

$$a_i(\nu) \rightrightarrows g_i(\nu) = K_i \frac{1}{\pi} \frac{\Gamma_i}{(\nu - \nu_{0i})^2 + \Gamma_i^2} \qquad (5)$$

The best fitted Lorentzian function reproduced the spectra fairly well, and the F_0, F_1, and F_2 values were obtained from the K_i values:

$$F_0 \cong (1/\tau_0) \int_{-\infty}^{\infty} g_0(\nu)\, \mathrm{d}\nu = (1/\tau_0) K_0$$
$$\text{and} \quad F_i \cong \int_{-\infty}^{\infty} g_i(\nu)\, \mathrm{d}\nu = K_i \; (i = 1, 2) \quad (6)$$

Then we were able to obtain the following ratios of the F_i values of the three fluorescing states: $F_0/F_1 = (1/\tau_0)(K_0/K_1) \approx 43$ and $F_1/F_2 = K_1/K_2 \approx 22$. The other parameters for the best fitted Lorentzian functions, the central frequency (ν_{0i}) and the half bandwidth (Γ_i), are as follows: $\nu_{00} = 2.30 \times 10^4$ cm^{-1} ($\lambda_{max} =$ 433 nm) and $\Gamma_0 = 1.2 \times 10^3$ cm^{-1} for the ultrafast component; $\nu_{01} = 2.24 \times 10^4$ cm^{-1} ($\lambda_{max} = 442$ nm) and $\Gamma_1 = 2.2 \times 10^3$ cm^{-1} for the fast component; $\nu_{02} = 1.73 \times 10^4$ cm^{-1} ($\lambda_{max} =$ 561 nm) and $\Gamma_2 = 3.1 \times 10^3$ cm^{-1} for the slow component.[43] Since the oscillator strength (f_i) is proportional to F_i/ν_{0i}^2, the ratios of the oscillator strengths of the three fluorescing states are also evaluated as $f_0/f_1 = (\nu_{01}/\nu_{00})^2(F_0/F_1) \approx 41$ and $f_1/f_2 = (\nu_{02}/\nu_{01})^2(F_1/F_2) \approx 13$.

3.3. Absolute Oscillator Strengths and Other Properties of the Fluorescing States. The absolute oscillator strength of the ultrafast fluorescing state was evaluated by comparing its time-resolved fluorescence intensity with that of a dye molecule. Figure 7 shows up-converted fluorescence decays at three different wavelengths obtained from a mixed hexane solution of *all-trans*-retinal ($c_r = 6.4 \times 10^{-4}$ mol dm^{-3}) and coumarin 153 ($c_c = 1.2 \times 10^{-4}$ mol dm^{-3}). The mixed solution was used to make the excitation and detection conditions exactly

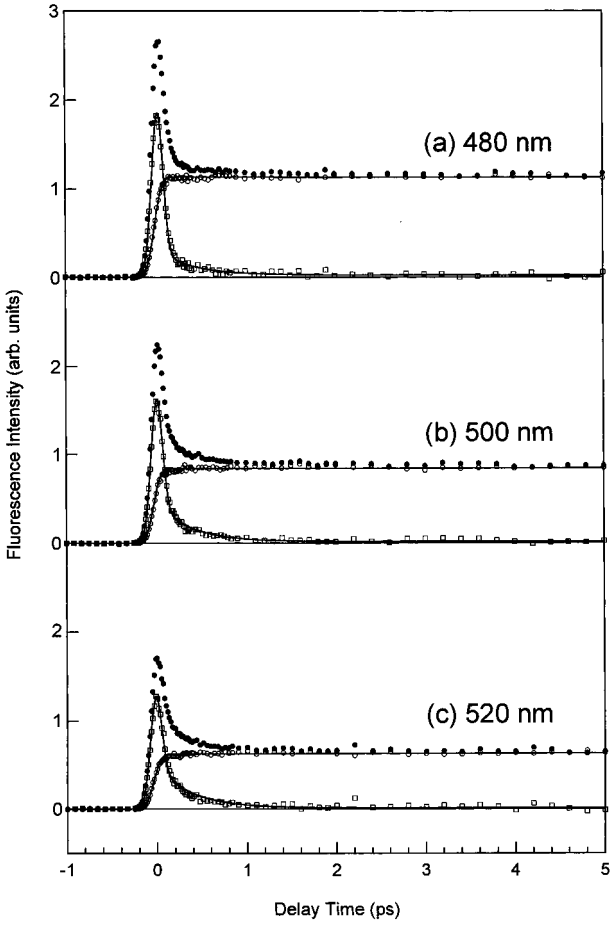

Figure 7. Comparison of the up-converted fluorescence decays obtained from a dye solution and a retinal-dye mixed solution at 480 (a), 500 (b), and 520 nm (c). (●) Fluorescence decays obtained from a mixed hexane solution of *all-trans*-retinal (6.4×10^{-4} mol dm^{-3}) and coumarin 153 (1.2×10^{-4} mol dm^{-3}). (○) Fluorescence decays obtained from a pure coumarin 153 solution (1.2×10^{-4} mol dm^{-3}). (□) Separated fluorescence decays of *all-trans*-retinal. Solid curves: calculated (see text).

the same for *all-trans*-retinal and the dye molecule. As shown in this figure, the observed fluorescence decays can be decomposed into the retinal fluorescence and the coumarin fluorescence, by using the fluorescence decay data obtained from a pure coumarin solution. The separated retinal contribution agrees very well with the fluorescence decay observed for pure retinal solution at each wavelength, implying that the excited state energy transfer and/or the complex formation are negligible in the mixed solution. In the measured time range, the fluorescence intensity of coumarin 153 is almost constant, so that its temporal behavior is represented as $R_c(t) = a_c$. In the same way as the discussion in the previous section, the quantity F_c is defined for the coumarin fluorescence, and then the ratio of the F_c and F_0 values can be related to the oscillator strengths of the fluorescing states of coumarin 153 (^1B_u state, $f_c = 0.39$[44]) and *all-trans*-retinal (the ultrafast fluorescing state, f_0):

$$\frac{F_0}{F_c} = \left(\frac{\nu_{00}}{\nu_{0c}}\right)^2 \left(\frac{f_0}{f_c}\right)\left(\frac{\epsilon_r c_r}{\epsilon_c c_c}\right) \qquad (7)$$

Here ϵ_r and ϵ_c are the extinction coefficients of the two molecules at the excitation wavelength of 400 nm ($\epsilon_r \approx \epsilon_c \approx 2 \times 10^4$ M^{-1} cm^{-1}). The factor of ϵc is introduced in this expression for taking account of the initial concentration difference of the two photoexcited molecules. With use of the approximation given in formula 5, the left side of formula 7 can be also expressed as follows:

$$\frac{F_0}{F_c} = \frac{1}{\tau_0}\frac{K_0}{K_c} = \left(\frac{a_0(\nu_{obs})/\tau_0}{a_c(\nu_{obs})}\right)\left(\frac{\Gamma_c}{\Gamma_0}\right)\left[\frac{(\nu_{obs} - \nu_{00})^2 + \Gamma_0^2}{(\nu_{obs} - \nu_{0c})^2 + \Gamma_c^2}\right] \qquad (8)$$

where ν_{obs} is the frequency corresponding to the observation wavelength. The parameters for the best fitted Lorentzian function for the retinal ultrafast component were already given, while those for the coumarin fluorescence were $\nu_{0c} = 2.23 \times 10^4$ cm^{-1} and $\Gamma_c = 1.6 \times 10^3$ cm^{-1}.[45] Combining formulas 7 and 8, we can evaluate the oscillator strength of the ultrafast fluorescing state of *all-trans*-retinal (f_0) using its lifetime ($\tau_0 =$ 30 fs) and the a_0 and a_c values obtained from the fluorescence data in Figure 7. The value of $a_0/a_c = 0.244$ is obtained from the fluorescence data at 480 nm ($\nu_{obs} = 2.08 \times 10^4$ cm^{-1}), which gives the oscillator strength of $f_0 = 0.97$. The very similar values of $f_0 = 1.08$ and 1.05 are obtained from the fluorescence data at 500 and 520 nm, respectively. From this agreement of the f_0 values obtained at three different observation wavelengths, the oscillator strength of the ultrafast fluorescing state is safely evaluated as $f_0 = 1.0$.

The ratios of the oscillator strengths of the three fluorescing states have been already determined in the previous section. Thus we can obtain the absolute oscillator strengths of the other two states from the value of the ultrafast fluorescing state ($f_0 =$ 1.0): $f_1 = f_0/(f_0/f_1) \approx 1.0/41 = 0.024$ and $f_2 = f_1/(f_1/f_2) \approx 0.024/13 = 0.0018$. The radiative lifetimes of the three fluorescing states are also calculated on the basis of these oscillator strengths, and they are $\tau_{r0} \approx 2.8$ ns,[46] $\tau_{r1} \approx 120$ ns, and $\tau_{r2} \approx 2.8$ μs at each fluorescence frequencies (ν_{0i}). Corresponding extinction coefficients at the absorption maximum are $\epsilon_1 \approx 800$ M^{-1} cm^{-1} (the fast component) and $\epsilon_2 \approx 40$ M^{-1} cm^{-1} (the slow component), if we assume the same band shape for absorption and fluorescence and use the best fitted Lorentzian band shapes given in formula 5. The fluorescence quantum yield for each component can be also calculated as $\phi_0 = \tau_0/\tau_{r0} =$ 30 fs/2.8 ns $\approx 1 \times 10^{-5}$, $\phi_1 = \tau_1/\tau_{r1} \approx 0.3 \times 10^{-5}$, and $\phi_2 = \tau_2/\tau_{r2} \approx 1 \times 10^{-5}$, and then the total fluorescence quantum yield is given as $\phi_f = \phi_0 + \phi_1 + \phi_2 \approx 2 \times 10^{-5}$. This calculated quantum yield is consistent with the reported value ($\phi_f < 1 \times 10^{-4}$).[4,37,42] These evaluated characteristics of the three fluorescing states are listed in Table 1.

TABLE 1: Assignments and Properties of the Three Fluorescence Decay Components

	component		
	ultrafast	fast	slow
origin	^1B_u	^1A_g	$^1n\pi^*$
peak wavelength (nm)	430	440	560
lifetime (ps)	0.030 ± 0.015	0.37 ± 0.02	33−34[a]
oscillator strength	1.0	0.024	0.0018
radiative lifetime (ns)[b]	2.8	120	2800
fluorescence quantum yield (10^{-5})	1	0.3	1

[a] Reference 38. [b] Calculated for the transition frequencies at the fluorescence maximum.

3.4. Assignments of the Fluorescing States. In the singlet manifold of *all-trans*-retinal, there exist three low-lying electronically excited states, i.e., ^1B_u ($^1\pi\pi^*$), ^1A_g ($^1\pi\pi^*$), and $^1n\pi^*$ states. The ^1B_u state is an optically allowed state, and the strong ground-state absorption around 370 nm is due to the transition to this excited state. The ^1A_g state has a doubly excited nature, and the one-photon transition between the ground state and the ^1A_g state is symmetrically forbidden. In many polyenes, the

^1A_g state has lower energy than that of the ^1B_u state, being the lowest excited singlet state.[32,33] The $^1n\pi^*$ state originates from the carbonyl group. This state is also optically forbidden because the nonbonding orbital localized on the oxygen atom has a poor overlap with the antibonding π^* orbital. We discuss assignments of the three fluorescing states appearing after the photoexcitation, keeping these three excited singlet states in mind. As described below, the properties evaluated in the preceding sections (oscillator strength, radiative and fluorescence lifetimes, and excitation energy) strongly support the assignment that the fluorescence components are due to the three excited singlet states of *all-trans*-retinal, even though the other possibilities, such as the inhomogeneous distribution of the molecules or the contribution from small amount of the 13-*cis* isomer might not be ruled out completely.

Ultrafast Fluorescing State. The evaluated oscillator strength of the ultrafast fluorescing state ($f_0 = 1.0$) agrees very well with the reported value for the optically allowed ^1B_u state (1.18 ± 0.05[47]). Therefore, it is concluded that the ultrafast decay component arises from the initially populated ^1B_u state of *all-trans*-retinal. It should be noted that this very good agreement in oscillator strength strongly supports the reliability of the lifetime of 30 fs evaluated for the ultrafast fluorescing state.

Slow Fluorescing State. The fluorescing state corresponding to the slow decay component exhibits very weak fluorescence with the intensity maximum around 560 nm. The lifetime of 33−34 ps is in very good agreement with the reported rise-time of the triplet−triplet absorption[21,23,24,39] (most probably $T_7 \leftarrow T_1$ transition[48]), indicating that this state is the precursor of the lowest excited triplet state (T_1). In addition, the very weak fluorescence intensity suggests that this state is optically forbidden. Thus the slow decay component has been ascribed to the fluorescence from the optically forbidden lowest excited singlet state (S_1).[38]

The ^1A_g ($^1\pi\pi^*$) state and the $^1n\pi^*$ state are two candidates for the optically forbidden S_1 state. Of these two states, the $^1n\pi^*$ state is highly likely assigned to the S_1 state with consideration on the intersystem crossing (ISC) efficiency of *all-trans*-retinal. There is a well-known rule on relationship between the ISC efficiency and the electron configuration of the excited states: the ISC between the excited states with different electron configurations ($^1n\pi^* \leftrightarrow {}^3\pi\pi^*$, $^1\pi\pi^* \leftrightarrow {}^3n\pi^*$) takes place efficiently, while that between the same configurations ($^1n\pi^* \leftrightarrow {}^3n\pi^*$, $^1\pi\pi^* \leftrightarrow {}^3\pi\pi^*$) is, in principle, prohibited. This rule, the El-Sayed rule, was originally derived from the evaluation of the spin−orbit coupling matrix element[49,50] and has been widely accepted. It is known that the ISC between the states with the same electron configurations occurs typically with a time constant as long as 100 ns[51] while that between different configurations proceeds several orders of magnitude faster.[49,50] In the case of *all-trans*-retinal in hexane, the S_1 state is converted to the T_1 state with a time constant of 33−34 ps, and the ISC quantum yield is as high as 0.5.[52,53] This efficient ISC implies that the S_1 state and the T_1 state have different electron configurations. Since the T_1 state has been experimentally determined to be $^3\pi\pi^*$ state[54,55] it can be concluded that the S_1 state is the $^1n\pi^*$ state, not the ^1A_g state with $\pi\pi^*$ nature. This argument is consistent with inefficient ISC in retinol (vitamin A) and protonated Schiff base of retinal,[12,54] in which the $^1n\pi^*$ state can not take part in the ISC.

The absorption spectra of polyene aldehydes, $CH_3-(CH{=}CH)_n-CHO$ ($n \leq 4$), show that the $^1n\pi^*$ state is located at energies lower than those of the optically allowed ^1B_u state.[56] Although it is difficult to determine the energy of the $^1n\pi^*$-state of *all-trans*-retinal directly from its absorption spectrum, the $^1n\pi^*$ state should be located below the ^1B_u state because the nonplanarity between the ring double bond and the polyene side chain makes the effective conjugation length, *n*, less than five.[57] It is also noteworthy that the oscillator strength determined for the slow fluorescing state (0.0018) is comparable to the value reported for the $^1n\pi^*$ states of some polyene aldehydes (≈ 0.0005).[58]

Fast Fluorescing State. As shown in Figure 6, the ultrafast and the fast decay components exhibit fluorescence spectra in the very similar wavelength region. Du and Fleming measured time-resolved fluorescence of a protein-bound retinyl chromophore in bacteriorhodopsin[9] and observed nonsingle-exponential decays. They discussed the obtained data in terms of the excited state dynamics occurring within the lowest excited singlet state. However, the ultrafast and the fast decay components observed for *free* retinal in the present study are not attributable to a single electronically excited state, because the fluorescence intensities are significantly different from each other ($F_0/F_1 \approx 43$). They should be assigned to two different electronic origins. The fluorescing state corresponding to the fast decay component is located at energy slightly lower than the ^1B_u state, and it has moderate optical transition probability from the S_0 state ($f_1 \approx 0.024$). This state is assigned to the ^1A_g state based on the following three grounds. Firstly, as for *all-trans*-retinal in EPA solvent at 77 K, two photon absorption spectroscopy revealed that the ^1A_g state is located 2400 ± 300 cm^{-1} below the ^1B_u state.[47] In addition, it was reported that one-photon absorption spectra of *all-trans*-retinal crystal at 4.2 K exhibit a shoulder peak assignable to the $^1A_g \leftarrow S_0$ transition around 3200 cm^{-1} below the strong $^1B_u \leftarrow S_0$ band.[59] Although there has been no report on the accurate energy of the ^1A_g state in solution at room temperature, it is highly likely that the ^1A_g state is located slightly below the ^1B_u state. Secondly, the oscillator strength obtained for the fast fluorescing state (0.024) is in fair agreement with that of the ^1A_g state (0.07) estimated from the two photon absorption data at 77 K.[47] Thirdly, the extinction coefficient of the $^1A_g \leftarrow S_0$ transition of a homologous polyenal of retinal, $CH_3-(CH{=}CH)_5-CHO$, was reported to be ≈ 1500 M^{-1} cm^{-1} in EPA solvent at 77 K.[56] This value is comparable to the estimated extinction coefficient of 800 M^{-1} cm^{-1} for the fast fluorescing state.

As described above, the three decay components found in the fluorescence up-conversion data are safely assigned to the fluorescences from the ^1B_u, ^1A_g, and $^1n\pi^*$ states, in the order of decreasing energy and of increasing fluorescence lifetime. This excited state ordering is indeed consistent with the results of a semiempirical molecular orbital calculation.[36] Recently, Yamaguchi and Hamaguchi measured femtosecond time-resolved absorption spectra of *all-trans*-retinal in hexane and found that the obtained spectra consist of three components.[39] They assigned the three to the absorption due to the two excited singlet states and T_1 state of all-*trans*-retinal. The excited singlet states found in their work are presumably assignable to the ^1B_u and ^1A_g states. Although the values first reported in their paper were significantly different, they recently obtained the lifetimes of 0.07, 0.5−0.6, and 31 ps with the refinement of their analysis.[60] These revised lifetimes are in good agreement with the values obtained in the present fluorescence study (0.03, 0.37, and 33−34) if the limited time-resolution of their experiments is taken into account.

3.5. Ultrafast Relaxation Dynamics of Photoexcited *all-trans*-Retinal. Figure 8 shows the schematic energy diagram of *all-trans*-retinal in hexane which has been clarified in the present study. The three excited singlet states, i.e., the ^1B_u, ^1A_g, and $^1n\pi^*$ states, are involved in the relaxation pathway of photoexcited *all-trans*-retinal. The relaxation process in the

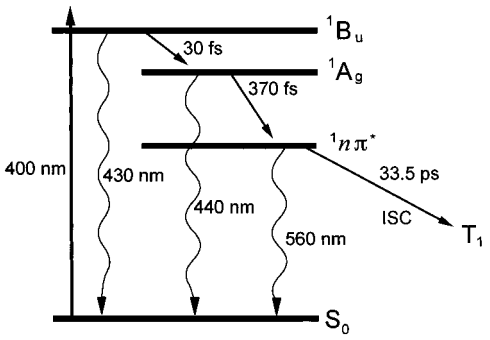

Figure 8. Schematic energy diagram illustrating the population relaxation pathway in the singlet manifold of *all-trans*-retinal after photoexcitation.

singlet manifold is described as follows. The photoexcitation at 400 nm first produces the dipole-allowed ^1B_u state. The initially prepared Franck−Condon state relaxes quite rapidly, and the relaxed ^1B_u state emits fluorescence around 430 nm. The fluorescence from the Franck−Condon state is not observed because its lifetime is in the order of the inverse of vibrational frequencies (<10 fs). The ^1B_u state then relaxes to the optically forbidden ^1A_g state with a time constant as short as 30 fs, and the ^1A_g state emits fluorescence around 440 nm. The very short internal conversion time from the ^1B_u state to the ^1A_g state reflects the small energy separation between these two excited states. In addition, the moderately strong fluorescence from the optically forbidden ^1A_g state indicates that there exists considerable mixing between the two states.[47] In other words, the ^1A_g fluorescence presumably takes place with intensity borrowing from the optically allowed ^1B_u state. The ^1A_g state is subsequently converted to the $^1n\pi^*$ state, which is the lowest excited singlet state, with a time constant of 370 fs. The $^1n\pi^*$ state is rigorously optically forbidden, and the $^1n\pi^*$ fluorescence appearing around 560 nm is much weaker than the ^1B_u fluorescence, or even than the ^1A_g fluorescence. Finally, the $^1n\pi^*$ state undergoes the efficient $^1n\pi^* \rightarrow {}^3\pi\pi^*$ ISC with a time constant of 33−34 ps to form the T_1 state. The low fluorescence quantum yield ($\phi_f \leq 1 \times 10^{-4}$) and high ISC yield ($\phi_{ISC} \approx 0.5$) of *all-trans*-retinal in hexane are attributable to the very short higher state lifetimes and the properties of the lowest excited $^1n\pi^*$ state. We note that the situation is quite different in polar hydrogen-bonding solvents. In these solvents, hydrogen-bonded retinal is formed and the ^1A_g state becomes the S_1 state in place of the $^1n\pi^*$ state. The change in the S_1 state character causes drastic changes in the triplet and fluorescence quantum yields: the triplet quantum yield falls to nearly zero,[12] and the fluorescence quantum yield jumps up to the order of 10^{-2}.[37] It is because the ^1A_g ($^1\pi\pi^*$) $\rightarrow {}^3\pi\pi^*$ ISC is very inefficient and because the $^1A_g \rightarrow S_0$ fluorescence transition probability is moderately large.

Acknowledgment. The authors acknowledge Prof. H. Hamaguchi and Mr. S. Yamaguchi of the University of Tokyo for sending us a preprint of their femtosecond visible absorption work on *all-trans*-retinal, as well as for giving us information about their recent analysis. The authors also thank Dr. A. Shimojima for his assistance in obtaining statinary fluorescence spectra of *all-trans*-retinal.

References and Notes

(1) Lanyi, J. K. *Bioenergetics*; Ernster, L., Ed., Elsevier: New York, 1984; Chapter 11.

(2) Hubbard, R.; Kropf, A. *Proc. Natl. Acad. Sci. U.S.A.* **1958**, *44*, 130.

(3) Wald, G. *Science* **1968**, *162*, 230.

(4) Becker, R. S. *Photochem. Photobiol.* **1988**, *48*, 369.

(5) Hochstrasser, R. M.; Johnson, C. K. *Ultrashort Laser Pulses and Applications*; Kaiser, W., Ed., Springer Verlag: New York, 1988; Chapter 9.

(6) Dobler, J.; Zinth, W.; Kaiser, W.; Oesterhelt, D. *Chem. Phys. Lett.* **1988**, *144*, 215.

(7) Mathies, R. A.; Brito Cruz, C. H.; Pollard, W. T.; Shank, C. V. *Science* **1988**, *240*, 777.

(8) Schoenlein, R. W.; Peteanu, L. A.; Mathies, R. A.; Shank, C. V. *Science* **1991**, *254*, 412.

(9) Du, M.; Fleming, G. R. *Biophys. Chem.* **1993**, *48*, 101.

(10) Kandori, H.; Sasabe, H. *Chem. Phys. Lett.* **1993**, *216*, 126.

(11) Kandori, H.; Katsuta, Y.; Ito, M.; Sasabe, H. *J. Am. Chem. Soc.* **1995**, *117*, 2669.

(12) Fisher, M. M.; Weiss, K. *Photochem. Photobiol.* **1974**, *20*, 423.

(13) Kropf, A.; Hubbard, R. *Photochem. Photobiol.* **1970**, *12*, 249.

(14) Raubach, R. A.; Guzzo, A. V. *J. Phys. Chem.* **1973**, *77*, 889.

(15) Rosenfeld, T.; Alchalel, A.; Ottolenghi, M. *J. Phys. Chem.* **1974**, *78*, 336.

(16) Waddell, W. H.; Crouch, R.; Nakanishi, K.; Turro, N. J. *J. Am. Chem. Soc.* **1976**, *98*, 4189.

(17) Waddell, W. H.; Hopkins, D. L. *J. Am. Chem. Soc.* **1977**, *99*, 6457.

(18) Hamaguchi, H. *Vibrational Spectra and Structure*; Durig, J. R., Ed.; Elsevier: New York; 1987; Vol. 116, Chapter 4, p 227 and references therein.

(19) Arai, T.; Tokumaru, K. *Chem. Rev.* **1993**, *93*, 23.

(20) Veyret, B.; Davis, S. G.; Yoshida, M.; Weiss, K. *J. Am. Chem. Soc.* **1978**, *100*, 3283.

(21) Hochstrasser, R. M.; Narva, D. L.; Nelson, A. C. *Chem. Phys. Lett.* **1976**, *43*, 15.

(22) Harriman, A.; Liu, R. S. H. *Photochem. Photobiol.* **1977**, *26*, 29.

(23) Hirata, Y.; Mataga, N.; Mukai, Y.; Koyama, Y. *Chem. Phys. Lett.* **1987**, *134*, 166.

(24) Mukai, Y.; Koyama, Y.; Hirata, Y.; Mataga, N. *J. Phys. Chem.* **1988**, *92*, 4649.

(25) Yuzawa, T.; Hamaguchi, H. *J. Mol. Struct.* **1995**, *352/353*, 489.

(26) Wilbrandt, R.; Jensen, N.-H. *J. Am. Chem. Soc.* **1981**, *103*, 1036.

(27) Atkinson, G. H.; Pallix, J. B.; Freedman, T. B.; Gilmore, D. A.; Wilbrandt, R. *J. Am. Chem. Soc.* **1981**, *103*, 5069.

(28) Hamaguchi, H.; Okamoto, H.; Tasumi, M. *Chem. Lett.* **1984**, 549.

(29) Hamaguchi, H.; Okamoto, H.; Tasumi, M.; Mukai, Y.; Koyama, Y. *Chem. Phys. Lett.* **1984**, *107*, 355.

(30) Wilbrandt, R.; Jensen, N.-H.; Levin, C. H. *Photochem. Photobiol.* **1985**, *41*, 175.

(31) Tahara, T.; Toleutaev, B. N.; Hamaguchi, H. *J. Chem. Phys.* **1994**, *100*, 786.

(32) Hudson, B. S.; Kohler, B. E. *Chem. Phys. Lett.* **1972**, *14*, 299.

(33) Hudson, B. S.; Kohler, B. E. *J. Chem. Phys.* **1973**, *59*, 4984.

(34) Christensen, R. L.; Kohler, B. E. *Photochem. Photobiol.* **1974**, *19*, 401.

(35) Das, P. K.; Becker, R. S. *J. Phys. Chem.* **1978**, *82*, 2081.

(36) Tallent, J. R.; Birge, J. R.; Zhang, C. F.; Wenderholm, E.; Birge, R. R. *Photochem. Photobiol.* **1992**, *56*, 935.

(37) Takemura, T.; Das, P. K.; Hug, G.; Becker, R. S. *J. Am. Chem. Soc.* **1978**, *100*, 2626.

(38) Tahara, T.; Hamaguchi, H. *Chem. Phys. Lett.* **1995**, *234*, 275.

(39) Yamaguchi, S.; Hamaguchi, H. *J. Mol. Struct.* **1996**, *379*, 87.

(40) The spectral resolution is predominantly determined by the monochromator slit width because the bandwidth of the up-conversion with the 0.5-mm-thick BBO crystal is larger. The spectral bandwidth of the gate pulse is not taken into consideration in this evaluation.

(41) Associated with the finite lifetime of the ultrafast component, a rise kinetics should be considered for the fast decay component. The inclusion of the rise kinetics does not affect the last functional form in foumula 1 but changes only the amplitude of the ultrafast component, a_0, from $a_0 = A_0$ to $a_0 = A_0 + \tau_0 a_1 = A_0 + 0.03a_1$. However the correction term $0.03a_1$ is so small that we were able to neglect it.

(42) Takemura, T.; Das, P. K.; Hug, G.; Becker, R. S. *J. Am. Chem. Soc.* **1976**, *98*, 7099.

(43) The λ_{max} values were determined as the peak wavelengths of the best fitted Lortentzian functions represented *in the λ-space*.

(44) This oscillator strength was calculated by integration of the absorption spectrum of coumarin 153 in hexane from 2.00×10^4 cm^{-1} (500 nm) to 3.33×10^4 cm^{-1} (300 nm).

(45) Maroncelli, M.; Fleming, G. R. *J. Chem. Phys.* **1987**, *86*, 6221.

(46) If the transition frequency at the absorption maximum (2.71×10^4 cm^{-1}) is used in this calculation instead of that at the fluorescence maximum ($\nu_{00} = 2.30 \times 10^4$ cm^{-1}), the radiative lifetime of $\tau_{r0} = 2.0$ ns is obtained.

(47) Birge, R. R.; Bennett, J. A.; Hubbard, L. M.; Fang, H. L.; Pierce, B. M.; Kliger, D. S.; Leroi, G. E. *J. Am. Chem. Soc.* **1982**, *104*, 2519.

(48) Becker, R. S.; Inuzuka, K.; King, J.; Balke, D. E. *J. Am. Chem. Soc.* **1971**, *93*, 43.

(49) El-Sayed, M. A. *J. Chem. Phys.* **1962**, *36*, 573.
(50) El-Sayed, M. A. *J. Chem. Phys.* **1963**, *38*, 2834.
(51) Abrahamson, E. W.; Adams, R. G.; Wulff, V. J. *J. Phys. Chem.* **1959**, *63*, 441.
(52) Bensasson, R.; Land, E. J.; Truscott, T. G. *Photochem. Photobiol.* **1975**, *21*, 419.
(53) Das, P. K.; Becker, R. S. *J. Am. Chem. Soc.* **1979**, *101*, 6348.
(54) Dawson, W.; Abrahamson, E. W. *J. Phys. Chem.* **1962**, *66*, 2542.
(55) Ros, M.; Hogenboom, M. A.; Kok, P.; Groenen, E. J. J. *J. Phys. Chem.* **1992**, *96*, 2975.
(56) Das, P. K.; Becker, R. S. *J. Phys. Chem.* **1982**, *86*, 921.
(57) Stam, C. H.; MacGillavry, C. H. *Acta Crystallogr.* **1963**, *16*, 62.
(58) Birge, R. R.; Leemakers, P. A. *J. Am. Chem. Soc.* **1972**, *94*, 8105.
(59) Drikos, G.; Morys, P.; Ruppel, H. *Photochem. Photobiol.* **1984**, *40*, 133.
(60) Yamaguchi, S.; Hamaguchi, H. Private communication.